JOURNAL OF AIRCRAFT
Vol. 57, No. 2, March–April 2020

Aeroelastics Flight Dynamics Coupling Effects of the Semi-Aeroelastic Hinge Device

A. Castrichini* and T. Wilson†
Airbus Operations, Ltd., Filton, England BS99 7AR, United Kingdom
F. Saltari,‡ F. Mastroddi,§ and N. Viceconti¶
University of Rome "La Sapienza", 00184 Rome, Italy
and
J. E. Cooper**
University of Bristol, Bristol, England BS8 1TH, United Kingdom

https://doi.org/10.2514/1.C035602

A recent consideration in aircraft design is the use of folding wingtips, with the aim of enabling higher-aspect-ratio aircraft with less induced drag but also meeting airport gate limitations. This study investigates the impact of floating folding wingtips on the aircraft flight dynamics. It is found that a floating wingtip aircraft has similar handling qualities with respect to an aircraft with no wing extension.

Nomenclature

b_j	=	gust spanwise shape function
b_l	=	aerodynamic lag pole
$C_{()}$	=	aerodynamic coefficient
c	=	mean aerodynamic chord
D	=	damping matrix
D_I	=	inertial damping
$\boldsymbol{e_1}, \boldsymbol{e_2}, \boldsymbol{e_3}$	=	practical mean axis reference versors
$\mathrm{F}_{\mathrm{Aero}}$	=	aerodynamic forces vector
g	=	gravity acceleration
H	=	gust gradient
J	=	inertia tensor
K	=	stiffness matrix
K_W	=	inertial stiffness
K_θ	=	torsional spring stiffness
k	=	reduced frequency
L_g	=	gust length
M	=	mass matrix, Mach number
M_{Hinge}	=	hinge moment
m	=	aircraft mass
Q_e	=	external forces
$Q_{i()}$	=	coefficient matrices of rational fraction approximation
$Q_{()}$	=	generalized aerodynamic force matrices
q_{dyn}	=	dynamic pressure
q_f	=	elastic modal displacement
r_l	=	aerodynamic states vector
S	=	reference wing area
T	=	aerodynamic transformation matrix from inertial reference to practical mean axis
T_1	=	transformation matrix from practical mean axis to inertial reference
$\boldsymbol{u}$	=	nodal displacement
u, v, w	=	aircraft velocity components in the practical mean axis
V	=	unperturbed air speed
v_{cg}	=	aircraft velocity in the practical mean axis
w_g	=	gust velocity
w_{g0}	=	peak of the gust velocity
w_j	=	gust vector
$\mathrm{w}_{\mathrm{ref}}$	=	reference gust velocity
$\boldsymbol{x}$	=	position in undeformed configuration
x_{cg}	=	aircraft center of mass position
x_j	=	jth panel's control node position
x_0	=	gust origin position
α	=	angle of attack
γ_j	=	jth panel's dihedral angle
δ_{tj}	=	Kronecker delta
δ_x	=	aerodynamic control surfaces vector
θ	=	wingtip folding angle
ξ	=	generalized coordinate
Φ	=	modal base
ψ	=	vector of the Euler angles
ω	=	angular velocity in the practical mean axis

Subscript

e	=	equilibrium value

Superscripts

$\dot{}$	=	differentiation with respect to time
$\sim$	=	Fourier transform
$\hat{}$	=	skew-symmetric matrix
$'$	=	variable in the inertial reference system

Received 20 May 2019; revision received 13 October 2019; accepted for publication 14 October 2019; published online 27 November 2019.

*Loads and Aeroelastics Engineer.
†Head of Technical Capability for Aircraft Loads Flight Physics.
‡Research Associate, Department of Mechanical and Aerospace Engineering.
§Associate Professor, Department of Mechanical and Aerospace Engineering.
¶Master Student, Department of Mechanical and Aerospace Engineering.
**Airbus Royal Academy of Engineering Sir George White Chair in Aerospace Engineering. Fellow AIAA.

I. Introduction

MUCH effort has been made to design aircraft to optimize fuel consumption through the reduction of aerodynamic drag. A sizable contribution (usually 30–40%) to the overall drag is lift-induced drag, which could be reduced by increasing the wingspan, but such a design solution has well-defined limits imposed by the maximum aircraft dimensions allowed at airports, as well as the increase in bending moments along the wing. A possible solution to the first issue is the use of folding wings that can be employed on the ground, similar to the retractable wings used on aircraft-carrier-borne aircraft. The inclusion of such a design feature raises the question as

to whether such a folding device could also be used to enable load reduction on the aircraft during the flight.

Recent works [1–5] have been aimed at studying the benefits of using a flexible wing-fold device for load alleviation and considering how it would be implemented on civil jet aircraft. The main idea consists of introducing a hinge in order to allow the wingtips to rotate, and it is known that the orientation of the hinge line relative to the airflow is a key parameter to enable successful load alleviation. When the hinge line is rotated outboard of the streamline, folding the wingtip up introduces a decrease in the local angle of attack [1]; such an effect provides a means to reduce the loads acting on the wing, leading to the possibility of achieving a wingtip extension with limited or even minimal impact on wing weight. Previous works have demonstrated that a free hinge is necessary in order to maximize the load alleviation performance [1]. However, zero hinge stiffness leads the wingtip to be deflected during straight and level cruise flight due to the static trim loads and, furthermore, to a continuous oscillating motion due to unsteady aerodynamic loads. Such deflections and continuous motions are undesirable because they will be detrimental to the aerodynamic performance and may lead to undesired rigid-body dynamic motion. Ideally, the wingtip should not deflect during cruise but only operate once a significant gust is encountered. Such a concept is called semi-aeroelastic hinge (SAH). During the cruise, the wingtip is kept in place by using a dedicated blocking mechanism. When a triggering event is detected, the wingtip is actively released and the tip device then acts as a passive load alleviation system, which is purely driven by the aerodynamic and inertial forces. After the load event is finished, an actuator is then engaged to bring back the wingtip to the initial clean configuration.

Previous works [1–5] focused on the impact of the SAH on the loads and flutter stability of a typical commercial jet aircraft. Now, an investigation is made on the mutual influence between the aeroelastic effect of the wingtip and the aircraft flight dynamics.

II. Aeroelastic Model

A. Practical Mean Axis Reference Frame

Typical aeroelastic equations of motion (EOMs) can be cast in the time domain as

$$
\begin{aligned}
&M\ddot{\xi}' + D\dot{\xi}' + K\xi' = Q'_e + F'_{\text{Aero}}\\
&\begin{bmatrix} mI & 0 & 0\\ 0 & J & 0\\ 0 & 0 & \bar{M}_{ff}\end{bmatrix}\begin{Bmatrix}\ddot{x}_{\text{cg}}\\ \ddot{\boldsymbol{\psi}}_{\text{cg}}\\ \ddot{q}_f\end{Bmatrix} + \begin{bmatrix} 0 & 0 & 0\\ 0 & 0 & 0\\ 0 & 0 & \bar{D}_{ff}\end{bmatrix}\begin{Bmatrix}\dot{x}_{\text{cg}}\\ \dot{\boldsymbol{\psi}}_{\text{cg}}\\ \dot{q}_f\end{Bmatrix}\\
&+\begin{bmatrix} 0 & 0 & 0\\ 0 & 0 & 0\\ 0 & 0 & \bar{K}_{ff}\end{bmatrix}\begin{Bmatrix}x_{\text{cg}}\\ \boldsymbol{\psi}_{\text{cg}}\\ q_f\end{Bmatrix} = \begin{Bmatrix}\bar{Q}_{e_x}\\ \bar{Q}_{e_{\boldsymbol{\psi}}}\\ \bar{Q}_{e_f}\end{Bmatrix} + \begin{Bmatrix}\bar{F}_{\text{Aero}_x}\\ \bar{F}_{\text{Aero}_{\boldsymbol{\psi}}}\\ \bar{F}_{\text{Aero}_f}\end{Bmatrix}
\end{aligned}
\tag{1}
$$

where M, D, and K are the generalized mass, damping, and stiffness matrices; Q'_e collects the non aerodynamic external generalized forces (i.e., gravity); F'_{Aero} are the generalized aeroelastic forces; and ξ' are the generalized displacements given by the aircraft center of gravity position x_{cg}, the aircraft Euler angles ψ_{cg}, and the elastic modal displacements q_f. These latter are related to a set of unconstrained mode shapes used to represent the linearized aircraft structural dynamics.

Several integrated models of flight dynamics and aeroelasticity have been proposed in the literature [6–11]. This work builds upon a simplified version of the formulation proposed by Saltari el al. [6]. The rigid-body degrees of freedom are here associated with a set of practical mean axes (PMAs). Such a reference has its origin at the instantaneous aircraft center of mass, but the orientation is fixed to the mean axes at the undeformed configuration. The rigid-body modes have to represent unitary translations x_{cg} and rotations ψ_{cg} around the aircraft center of mass at the undeformed configuration. The set of eigenvectors $\Phi$is taken as consistent, with the velocities and angular velocities defined positive in flight dynamics (e.g., a positive forward speed), allowing a better comprehension of the results concerning the rigid-body variables.

The structural physical displacements $\boldsymbol{u}$ are expressed on a modal basis as

$$
\boldsymbol{u}(\boldsymbol{x}, t) = \sum_{n=1}^{N_{\text{Modes}}} \Phi(\boldsymbol{x})\xi'(t) \tag{2}
$$

This kind of formulation introduces a significant approximation because only a limited number of structural modes are used. It is worth noting that the local accuracy of physical quantities having relevant space gradients (i.e., stress at the wing root) is highly dependent on the number of modes included in the analysis.

B. Inertial Modeling

Inertial coupling effects are generally considered of secondary importance [6] as compared to the effects provided by the aerodynamics and have been partially neglected here. However, in the general formulation of integrated flight dynamics and aeroelasticity, one may consider the rigid-body equations of motion expressed with respect to a noninertial frame of reference. In an aeroelastic framework, the rigid-body motion is expressed with respect to the finite element model (FEM) frame, moving in a uniform rectilinear motion with respect to the inertial frame. Thus, some further inertial and weight projection effects arise. More specifically, the absolute acceleration and angular momentum can be expressed with respect to the noninertial frame of reference attached to the PMAs:

$$
\begin{aligned}
\frac{D\boldsymbol{v}_{\text{cg}}}{Dt} &= \dot{\boldsymbol{v}}_{\text{cg}} + \boldsymbol{\omega}\times\boldsymbol{v}_{\text{cg}} \simeq \Delta\dot{\boldsymbol{v}}_{\text{cg}} - \boldsymbol{v}_{\text{cg}_e}\times\Delta\boldsymbol{\omega}\\
\frac{D(\boldsymbol{J\omega})}{Dt} &= \boldsymbol{J}\dot{\omega} + \boldsymbol{\omega}\times\boldsymbol{J\omega} \simeq \boldsymbol{J}\Delta\dot{\boldsymbol{\omega}}
\end{aligned}
\tag{3}
$$

where $\boldsymbol{v}_{\text{cg}}$ and $\boldsymbol{\omega}$ are the velocity and angular velocity physical entities, whereas $\boldsymbol{J}$ is the inertia tensor.

For a linearized analysis, the components of angular velocity $\boldsymbol{\omega}$ coincide with the derivative of Euler angles $\Delta\boldsymbol{\psi}$. On the other hand, the component of $\boldsymbol{v}_{\text{cg}}$ will be expressed in the noninertial frame of reference and be denoted as v_{cg}. The position of the body in the inertial frame of reference can thus be recast as

$$
\begin{aligned}
\Delta\dot{x}_{\text{cg}} &= \Delta v_{\text{cg}} - \hat{v}_{\text{cg}_e}\Delta\boldsymbol{\psi}\\
\dot{\xi}' &= \dot{\xi} + T_1\xi'
\end{aligned}
\tag{4}
$$

where

$$
T_1 = \begin{bmatrix} 0 & -\hat{v}_{\text{cg}_e} & 0\\ 0 & 0 & 0\\ 0 & 0 & 0\end{bmatrix}
$$

Summarizing the preceding concepts, the EOMs will be recast with respect to ξ and ξ', which are defined as

$$
\xi' = \begin{Bmatrix}\Delta x_{\text{cg}}\\ \Delta\boldsymbol{\psi}\\ \Delta q_f\end{Bmatrix}; \qquad \dot{\xi} = \begin{Bmatrix}\Delta v_{\text{cg}}\\ \Delta\omega\\ \Delta\dot{q}_f\end{Bmatrix}
$$

Skipping the intermediate passages for the sake of conciseness, the following damping matrix D_I allows us to switch the EOMs from the inertial frame to the noninertial frame in case of small perturbations around a steady rectilinear flight:

$$
D_I = \begin{bmatrix} 0 & -m\hat{v}_{\text{cg}_e} & 0\\ 0 & 0 & 0\\ 0 & 0 & 0\end{bmatrix} \tag{5}
$$

where v_{cg_e} is the trim speed vector.

Moreover, the description of the aircraft motion in the PMA noninertial reference requires accounting for the projection of the weight force on the aircraft body reference. Under the assumption of a small perturbation with respect to the trimmed configuration, such a contribution is modeled as an additional stiffness term to be added to $\bar{K}$, and defined as

$$K_W = mg \begin{bmatrix} 0 & 0 & 0 & 0 & 1 & 0 & & \\ 0 & 0 & 0 & -1 & 0 & 0 & \cdots & 0 \\ 0 & 0 & 0 & 0 & 0 & 0 & & \\ \vdots & & & \vdots & & & \ddots & \vdots \\ & 0 & & & 0 & & \cdots & 0 \end{bmatrix} = \begin{bmatrix} 0 & m\hat{g} & 0 \\ 0 & 0 & 0 \\ 0 & 0 & 0 \end{bmatrix} \tag{6}$$

with mg as the weight of the aircraft.

C. Aerodynamic Modeling

Unsteady aerodynamic effects are modeled using the doublet lattice method (DLM) [12,13]. The same modal formulation employed to model the structural dynamics is used to describe the unsteady aerodynamic forces, which are therefore strongly dependent on the number of modes used. In the frequency domain, the DLM unsteady aerodynamic forces are defined as [13]

$$\tilde{F}'_{\text{Aero}} = q_{\text{dyn}}[Q'_{hh}(M,k)\tilde{\xi}'_h + Q'_{hx}(M)\tilde{\boldsymbol{\delta}}_x + Q'_{hj}(M,k)\tilde{\boldsymbol{w}}_j] \tag{7}$$

where Q'_{hh} ($N_{\text{Modes}} \times N_{\text{Modes}}$), Q'_{hx} ($\text{N}_{\text{Modes}} \times \text{N}_{\text{ControlSurf}}$), and Q'_{hj} ($N_{\text{Modes}} \times N_{\text{Panels}}$), are, respectively, the generalized aerodynamic force matrices related to the Fourier transform of the generalized coordinates $\tilde{\xi}'_h$, the control surfaces vector $\tilde{\delta}_x$, and the gust shape $\tilde{w}_j$; and q_{dyn} ($q_{\text{dyn}} = (1/2)\rho V^2$) is the dynamic pressure.

The gust vector defines the downwash on a generic aerodynamic panel j due to the gust such that

$$w_j = b_j(y)\cos\gamma_j \frac{w_{g0}}{2V}\left(1 - \cos\left(\frac{2\pi V}{L_g}\left(t - \frac{x_0 - x_j}{V}\right)\right)\right)\delta_{t_j} \tag{8}$$

where L_g is the gust length (twice the gust gradient H), δ_{t_j} is a Kronecker delta that is equal to one only in the time window when the gust crosses the jth panel

$$\left(\frac{x_0 - x_j}{V} \le t_j \le \frac{x_0 - x_j}{V} + \frac{V}{L_g}\right)$$

b_j is a shape function defining the gust spanwise shape, and w_{g0} is the peak gust velocity; the latter is defined (in meters per second) as [14]

$$w_{g0} = w_{\text{ref}}\left(\frac{H}{106.17}\right)^{(1/6)} \tag{9}$$

For computational efficiency, the Aerodynamic Influence Coefficient (AIC) (and therefore the Generalised Aerodynamic Forces (GAF)) matrices are generated for a limited set of reduced frequencies [$k = (\omega c/2V)$] and Mach numbers; the remaining intermediate values are evaluated through interpolation schemes [13].

As for the mass, damping, and stiffness, the aerodynamic matrices are also expressed in the PMA reference system. The DLM GAF matrices are formulated in the inertial reference system [12,13] under the assumption of steady longitudinal flight. As result of such a formulation, any variations of pitch angle or yaw are considered as equivalent variations of the aerodynamic angle of attack and sideslip, respectively. In the PMA reference formulation, instead, a static rotation of an aircraft does not generate any aerodynamic forces perturbation. Such a correction on the rigid-body aerodynamic forces is achieved by postmultiplying the Q'_{hh} matrix, which is expressed in the inertial frame of reference, with a transformation matrix T ($N_{\text{Modes}} \times N_{\text{Modes}}$) [6] such that

$$Q_{hh}(k,M) = Q'_{hh}(k,M)T(k) \tag{10}$$

where

$$T(k) = \begin{bmatrix} 1 & 0 & 0 & 0 & 0 & 0 & & \\ 0 & 1 & 0 & 0 & 0 & b/jk & & \\ 0 & 0 & 1 & 0 & b/jk & 0 & & \\ 0 & 0 & 0 & 1 & 0 & 0 & \cdots & 0 \\ 0 & 0 & 0 & 0 & 1 & 0 & & \\ 0 & 0 & 0 & 0 & 0 & 1 & & \\ & & \vdots & & & & \ddots & \vdots \\ & & 0 & & & & \cdots & 1 \end{bmatrix}$$

where the elastic modes related block is set equal to the identity matrix because the definition of the elastic modes of the system is kept unchanged.

The aerodynamic forces are then recast in a time domain formulation using the rational fraction approximation method proposed by Roger [15] such that

$$\begin{aligned} F_{\text{Aero}} = q_{\text{dyn}}\Bigg\{&\left[Q_{hh0}\xi'_h + \frac{c}{2V}Q_{hh1}\dot{\xi}_h + \left(\frac{c}{2V}\right)^2 Q_{hh2}\ddot{\xi}_h\right] \\ &+ [Q'_{hx0}\delta_x] + \left[Q'_{hj0}w_j + \frac{c}{2V}Q'_{hj1}\dot{w}_j\right. \\ &\left. + \left(\frac{c}{2V}\right)^2 Q'_{hj2}\ddot{w}_j\right] + \sum_{l=1}^{N_{\text{Poles}}} r_l\Bigg\} \end{aligned} \tag{11}$$

where r_l is the generic aerodynamic state vector related to the generic lag pole $b_l = (k_{\max}/l)$. These extra states allow the modeling of the unsteady response of the aerodynamics by taking into account of the delay of the aerodynamic forces with respect to the structural deformations. These aerodynamic states were evaluated through the set of dynamic equations

$$\dot{r}_l = -b_l\frac{2V}{c}Ir_l + Q_{hh2+l}\dot{\xi}_h + Q'_{hj2+l}\dot{w}_j, l = 1,\ldots,N_{\text{Poles}} \tag{12}$$

which are solved together with the equations of motion [Eq. (1)].

The matrices Q_{hh0}, Q_{hh1}, and Q_{hh2} have the physical meanings of the aerodynamic stiffness, damping, and inertia, respectively. The transformation introduced in Eq. (10) led to having the first six columns of Q_{hh0} equal to zero, meaning that no aerodynamic stiffness is associated with the rigid-body modes.

Further aerodynamic correction terms are also introduced to account for aerodynamic contributions that are, in general, neglected by the DLM, such as the aerodynamic drag. This latter contribution can be expressed as

$$D = q_{\text{dyn}}C_D = q_{\text{dyn}}S(C_{D_0} + C_{D_\alpha}\alpha) \tag{13}$$

The perturbation of the aerodynamic drag from the equilibrium value, due to a variation of the longitudinal velocity and angle of attack, can be obtained by linearizing Eq. (13) as

$$\begin{aligned} \left.\frac{\partial D}{\partial u}\right|_{D_e} &= \rho V S C_{D_e} = \frac{2q_{\text{dyn}}S}{V^2}C_{D_e} \\ \left.\frac{\partial D}{\partial \alpha}\right|_{D_e} &= \left.\frac{\partial D}{\partial \boldsymbol{w}}\right|_{D_e} = q_{\text{dyn}}SC_{D_\alpha} = \frac{q_{\text{dyn}}S}{V}C_{D_\alpha} \end{aligned} \tag{14}$$

and these terms represent the additional aerodynamic damping contributions that affect the longitudinal aircraft dynamics and can be collected in the damping matrix $Q_{hh1D}(N_{\text{Modes}} \times N_{\text{Modes}})$ [6] defined as

$$Q_{hh1D} = \begin{bmatrix} -2C_{D_e}S/c & 0 & -C_{D_\alpha}S/c & 0\,0\,0 & & \\ 0 & 0 & 0 & 0\,0\,0 & & \\ 0 & 0 & 0 & 0\,0\,0 & \cdots & 0 \\ 0 & 0 & 0 & 0\,0\,0 & & \\ 0 & 0 & 0 & 0\,0\,0 & & \\ 0 & 0 & 0 & 0\,0\,0 & & \\ & & \vdots & & \ddots & \vdots \\ & & 0 & & \cdots & 0 \end{bmatrix} \tag{15}$$

The DLM GAF matrices are evaluated at a zero angle of attack; however, the EOMs are linearized around a trimmed configuration, and hence the aerodynamics loads acting on an unconstrained aircraft should be corrected in order to account for the effects of a nonzero angle of attack. These quasi-steady effects are particularly relevant in flight dynamics in terms of rigid-body response and stability, and they are due to the aerodynamic forces introduced by a perturbation of dynamic pressure and angle of attack being a function of the equilibrium angle of attack. These contributions can be modeled by assuming that a perturbation of dynamic pressure results in a variation of the local lift magnitude, whereas a perturbation of the angle of attack reflects in a variation of the local lift direction. Both of these terms are evaluated by linearizing the trim aerodynamic forces distribution with respect to the longitudinal speed and angle of attack as

$$\Delta f_{\text{Aero}}(x,\,t) = -2\frac{f_{\text{AeroTrim}}(x,\,t)}{V}\Delta u(x,\,t) + f_{\text{AeroTrim}}(x,\,t)\cdot e_3\Delta\alpha(x,\,t)e_1 \tag{16}$$

Such a linearization results in the definition of further matrices $Q_{hh1\alpha}$ and $Q_{hh1q_{\text{dyn}}}$ being added to the aerodynamic stiffness matrix Q_{hh1}. Saltari et al. [6] provided further details on the derivation of these terms.

D. Final Formulation of Equations of Motion

A nonlinear reduced-order model is defined to model the linear and nonlinear hinge mechanisms.

The idea is to use the set of flexible modes obtained when a very low hinge spring stiffness is defined along the hinge line; a zero stiffness value was avoided to prevent numerical singularities during the modal analysis. This approach showed the first two flexible modes to be local symmetric and antisymmetric pseudorigid wingtips deflections, as shown in Figs. 1a and 1b. Such modal shapes are (by definition) orthogonal, with the remaining flexible modes involving a combination of wingtips and main airframe deformations (Figs. 1c and 1d); therefore, they could be used to describe independent wingtip rotations. The overall span reduction due to the wingtips deflection was not considered.

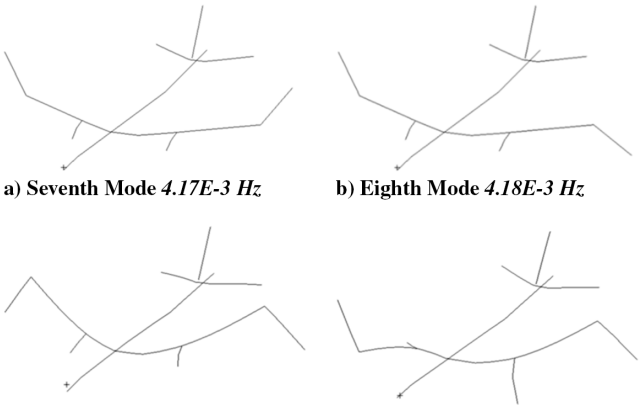

a) Seventh Mode *4.17E-3 Hz* **b) Eighth Mode *4.18E-3 Hz***

c) Ninth Mode *2.22E0 Hz* **d) 10th Mode *2.54E0 Hz***

Fig. 1 Typical flexible modes of an aircraft with the folding wingtips.

Linear and nonlinear hinge devices (such as springs, dampers, or actuators) can be modeled by applying external moments on the hinge nodes along the hinge axis in order to simulate the related restoring moments on the wingtips and main airframe, as shown in Fig. 2. The hinge moments could be defined as linear or nonlinear functions of the wingtip folding angle and, once projected onto the structural modes, defined as a set of generalized forces that could excite mainly the local wingtip modes, and so drive the wingtip motion.

The aerodynamic forces are given by

$$F_{\text{AeroTot}} = q_{\text{dyn}}\left\{\left[Q_{hh0}\xi_h' + \frac{c}{2V}(Q_{hh1} + Q_{hh1D} + Q_{hh1\alpha} + Q_{hh1q_{\text{dyn}}})\dot{\xi}_h + \left(\frac{c}{2V}\right)^2 Q_{hh2}\ddot{\xi}_h\right] + [Q_{hx0}'\boldsymbol{\delta}_x] + \left[Q_{hj0}'w_j + \frac{c}{2V}Q_{hj1}'\dot{w}_j + \left(\frac{c}{2V}\right)^2 Q_{hj2}'\ddot{w}_j\right] + \sum_{l=1}^{N_{\text{Poles}}} r_l\right\} \tag{18}$$

where the equations regulating the dynamics of the aerodynamic finite states are given by Eq. (12), and the final stiffness and damping matrices are expressed as

$$K_{\text{Tot}} = K + K_W \tag{19}$$

$$D_{\text{Tot}} = D + D_I \tag{20}$$

The linear and nonlinear hinge mechanisms are simulated through the introduction of the generalized nonlinear force M'_{Hinge}. The idea is to simulate a mechanism that allows the wingtip to rotate only when the aerodynamic forces are higher than some predefined threshold value. Such a device was modeled by applying, to the wingtips and main airframe, the restoring moments due to a piecewise linear spring for which the stiffness was varied according to the loads experienced by the aircraft such that

$$M_{\text{Hinge}} = -K_\theta\theta \quad \begin{cases} K_\theta = 1.E^{12}\ \text{N}\cdot\text{m/rad if } 0 < t < t_{\text{release}} \\ K_\theta = 1.E^{0}\ \text{N}\cdot\text{m/rad if } t \geq t_{\text{release}} \end{cases} \tag{21}$$

III. Numerical Results

A single-aisle aircraft linear structural model is used for the analyses. The wingtip extensions are connected to the main wing structure in a similar way as in previous work [1]. The total span is increased by roughly 25%. A single flight point was considered at 25,000 ft of altitude and a Mach number of $M = 0.82$.

A series of dynamic and static analyses have been performed in order to assess the open-loop response of an aircraft with free and fixed wingtips with respect to a baseline model without the tip extension. The three models have the same control surfaces. The three models share the same mass distribution for the fuselage, engines, tail planes, and inner wing. The same mass was assumed for the hinge mechanism and wingtips of free and fixed-hinge models to

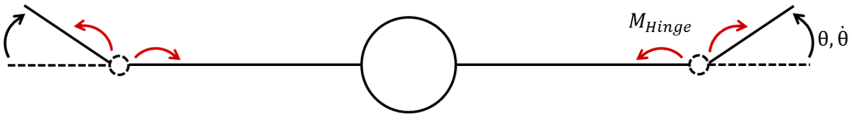

Fig. 2 Applied hinge moments.

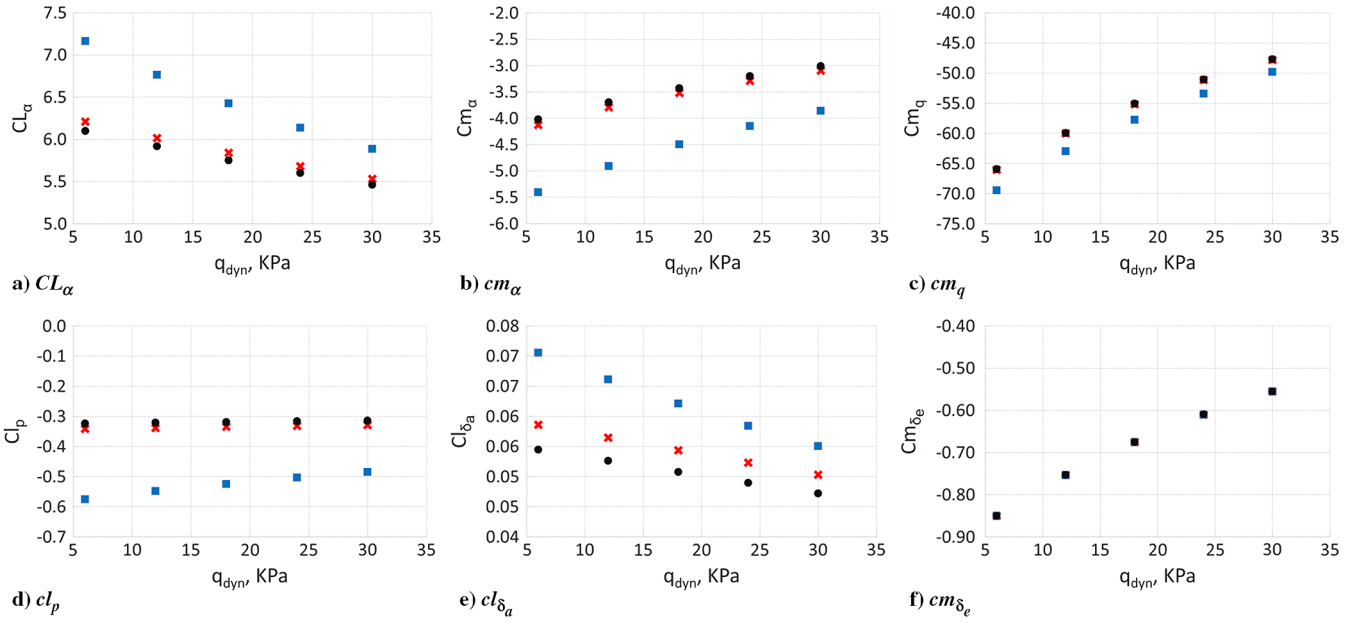

Fig. 3 Aerodynamic derivative: baseline (black dot); fixed hinge (blue square); and free hinge (red cross).

account for the fact that a wingspan extension would require, in any case, a hinge mechanism to allow the wing folding while on the ground.

A. Aerodynamic Derivatives and Handling Qualities

This section presents an investigation of the impact of the SAH on the aircraft aerodynamic derivatives and handling qualities. Figure 3 reports the variation of some aerodynamic derivatives for different dynamic pressure values. The aircraft with the free folding wingtip shows very close aerodynamic derivatives with respect to the baseline model. In terms of CL_α, this is easily justifiable by the fact that an increment of the angle of attack generates an upward deflection of the wingtip, resulting in negative incremental aerodynamic loads, and thus reducing the CL_α to the same level of the baseline aircraft with a smaller wing. The same comments are valid for Cm_α, which decreases passing from a fixed to a free hinge.

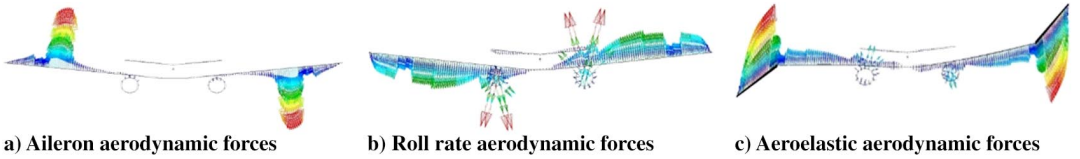

a) Aileron aerodynamic forces b) Roll rate aerodynamic forces c) Aeroelastic aerodynamic forces

Fig. 4 Aerodynamic forces contributions due to a rolling maneuver.

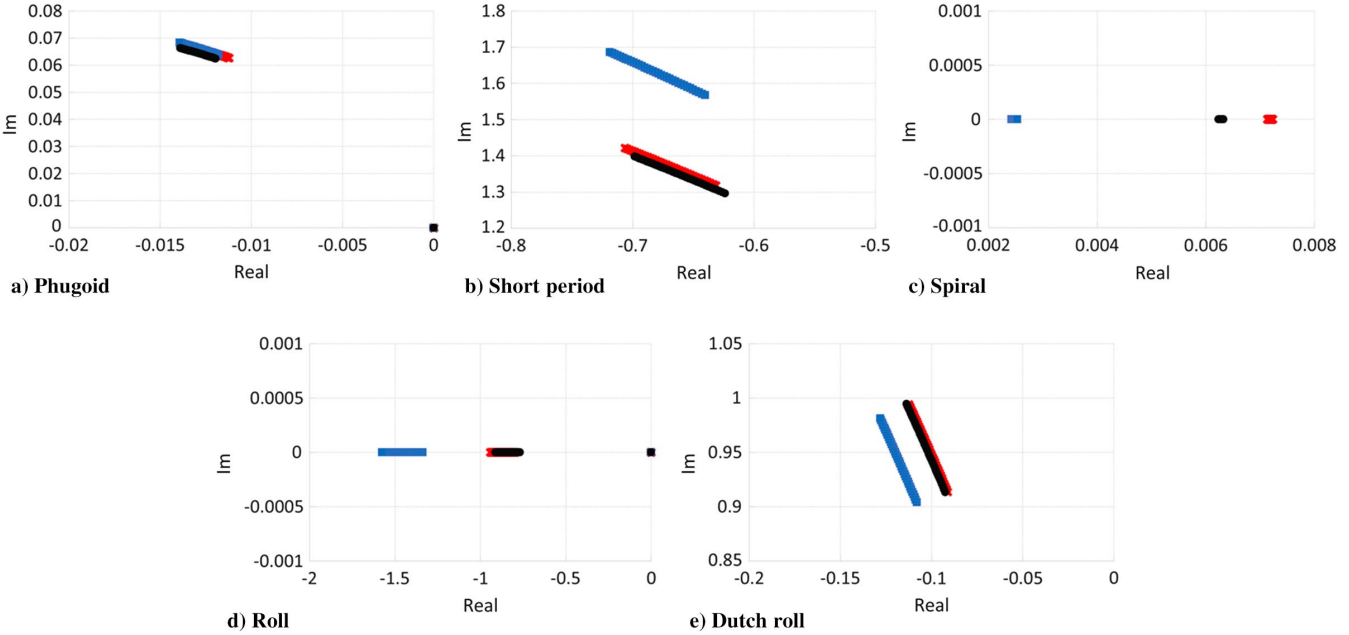

Fig. 5 Root locus: baseline (black dot); fixed hinge (blue square); and free hinge (red cross).

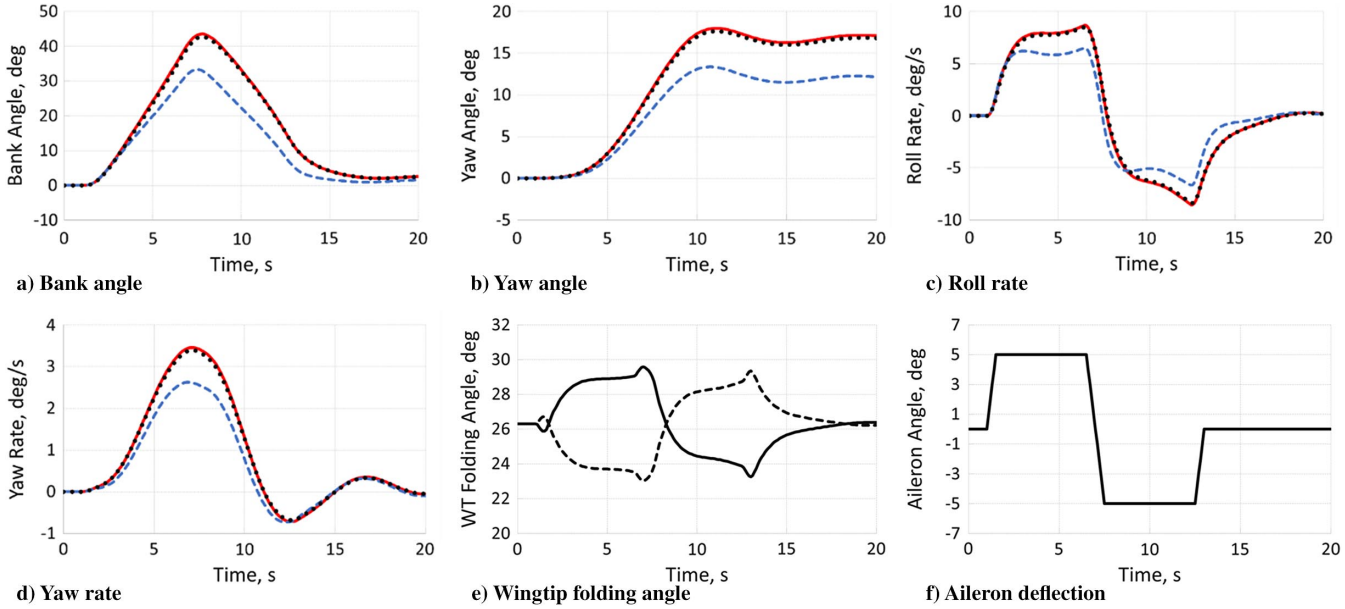

Fig. 6 Dynamic response due to an aileron deflection: baseline (black dotted line); fixed hinge (blue dashed line); and free hinge (red solid line).

A significant impact is observed in terms of rolling damping Cl_p between free and fixed wingtip configurations. A well-known problem associated to high-aspect-ratio wings is the reduction of rolling authority due to the increment of rolling damping introduced by the longer span. Having free wingtips seems to overcome this limitation, leading to comparable roll damping levels of an aircraft without the wing extension. Such an improvement of the rolling handling qualities can be explained by analyzing the aerodynamic forces generated during the maneuver. In the case of a positive roll maneuver, the right wing tends to go down, whereas the left wing goes up. The incremental aerodynamic forces induced by the roll rate will generate an incremental upward deflection of the right wingtip, whereas the left wingtip will see a reduction of the folding angle. The resulting rolling moment induced by the aeroelastic loads will have the same sense of the rolling moment induced by the aileron, as shown in Fig. 4. Moreover, the variation of the angle of attack introduced by the wingtip deflection is constant all over the tip surface, whereas the roll rate generates higher variation of the local angle of attack toward the tip. As a result, the wingtip deflection will generate an incremental lift contribution that is closer to the hinge with respect to the incremental lift induced by the roll rate. Because a perfect free hinge cannot pass any bending moment, such a condition is satisfied (neglecting the inertial terms) only if the local lift contribution due to the wingtip deflection is higher than the one due to the roll rate. As a consequence, the hinges see net shear forces that aid the rolling maneuver, thus increasing the rolling authority of the aileron.

Figure 3e shows the rolling moment coefficient introduced by the aileron. Despite the three models sharing the same aileron, different values are observed between the baseline and the free and the fixed-hinge aircraft, even for low dynamic pressure where the aeroelastic effects are less pronounced. This finding is due to the fact that the aileron is placed close to the hinge; as a consequence, for a longer-span aircraft, an aileron deflection will produce spill over aerodynamic forces that will also interest part of the tip, as shown in Fig. 4a. This would lead the local aileron center of pressure to move outboard, thus increasing the moment arm. Moreover, Fig. 3e shows that the rolling moment coefficient of the free wingtip aircraft has a lower gradient with respect to the fixed-hinge one, leading to a delay of the aileron reversal when the floating tips are employed. Such an

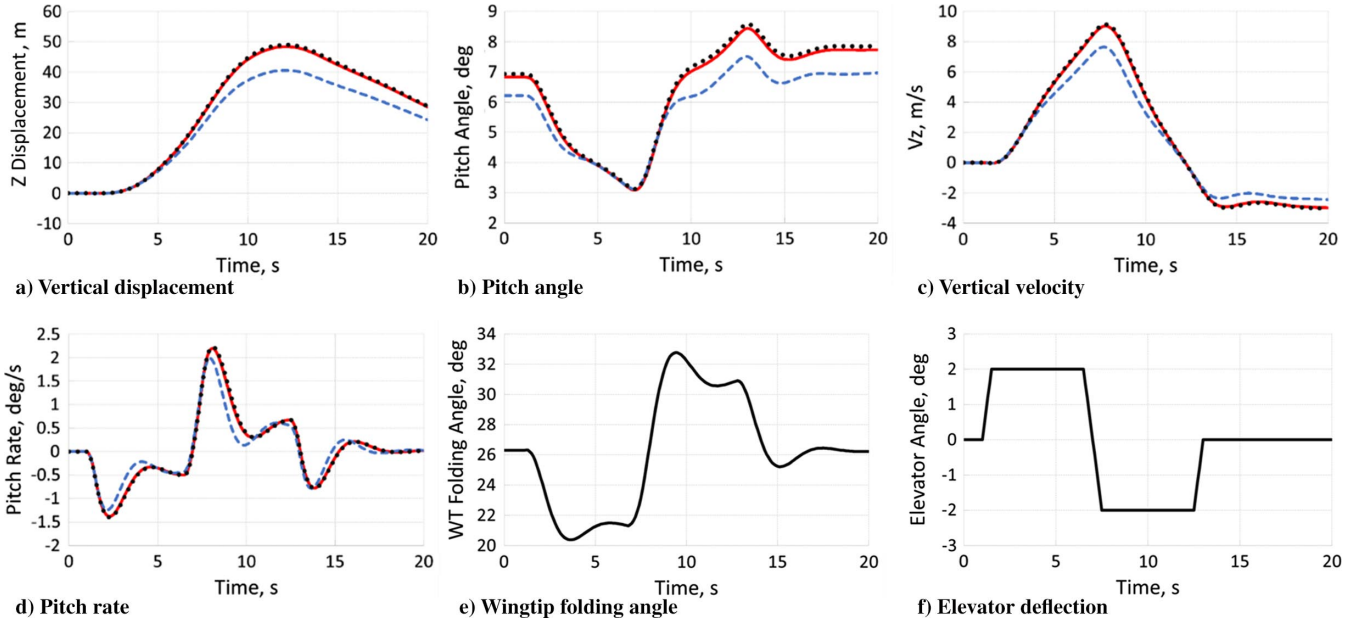

Fig. 7 Dynamic response due to an elevator deflection: baseline (black dotted line); fixed hinge (blue dashed line); and free hinge (red solid line).

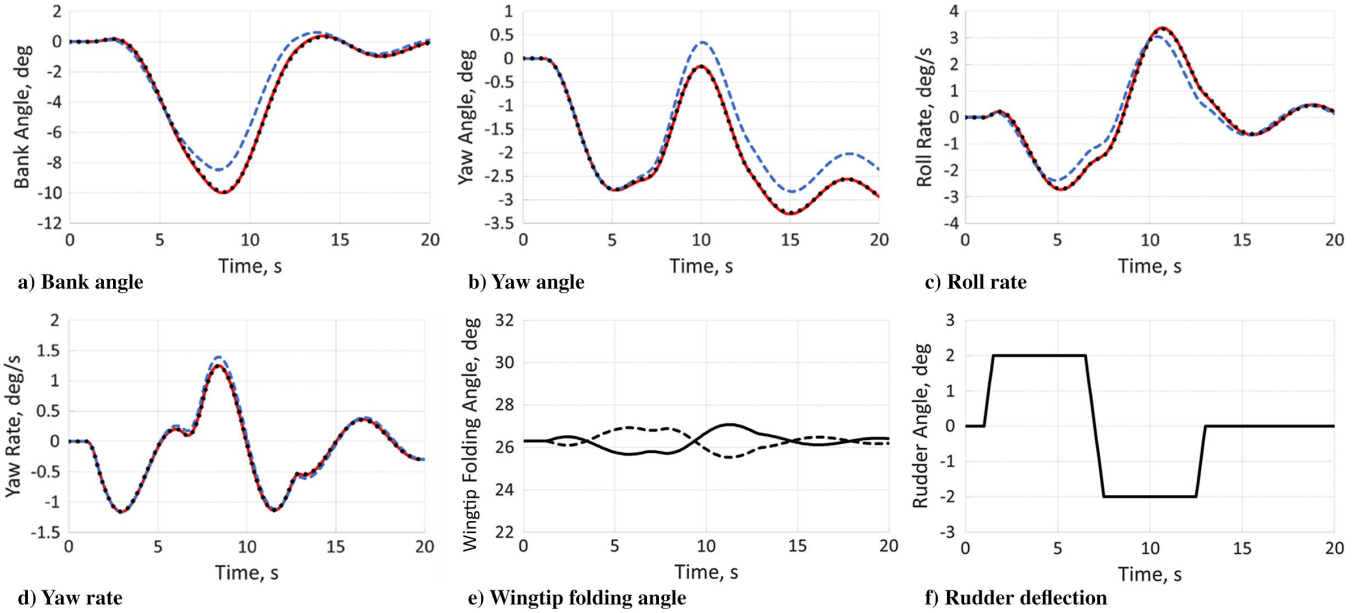

Fig. 8 Dynamic response due to a rudder deflection: baseline (black dotted line); fixed hinge (blue dashed line); and free hinge (red solid line).

effect is due to the fact that the aerodynamic forces produced by the tip's deflection tend to reduce the wing bending; this reflects in a reduction of the wing torsion in the case of a sweepback wing, and thus on a positive impact on the aileron reversal.

A small impact is also observed for Cm_q, whereas Cm_{δ_e} does not vary between the three aircraft.

Figure 5 reports the evolution of root locus of the aeroelastic system for different values of dynamic pressure; particular attention is given to the flight dynamics modes. No significant impact is observed for the long-period mode. As regards the short-period motion, a variation is observed between the fixed- and free-hinge aircraft, with the latter having almost the same values of the baseline condition. The three aircraft share similar values for the real part of the poles but with the fixed-hinge aircraft showing higher imaginary values. This finding indicates the three models have similarly damped short-period modes but with higher-frequency for the fixed-hinge case. The spiral mode is unstable for all the analyzed configurations. and the use of a free hinge seems to destabilize such dynamics even further. This is usually not a problem because many aircraft have an unstable spiral model, which can be easily stabilized with a proper control law. Regarding the roll and Dutch roll, there is almost no impact on the frequency, and a reduction of the damping is observed between the fixed- and free-hinge aircraft; this is in agreement with what is shown in Fig. 4d. Again, the free hinge shows values that are similar to the baseline ones.

B. Dynamic Maneuvers

In this section, a comparison is made between the free-hinge, fixed-hinge, and baseline model responses to time-varying commands on the aileron, elevator, and rudder, respectively.

Figure 6 shows the aircraft response to an aileron command. The command time history is shown in Fig. 6f. The plots show that the free-hinge aircraft has the same dynamic response of the baseline model, achieving a higher roll rate with respect to the fixed-hinge aircraft. This is in agreement with what has been shown in the previous section. Figure 6e reports the asymmetric wingtip deflection induced by the maneuver.

Figure 7 reports the dynamic response due to an elevator deflection. Again, the free-hinge aircraft shows the same response as

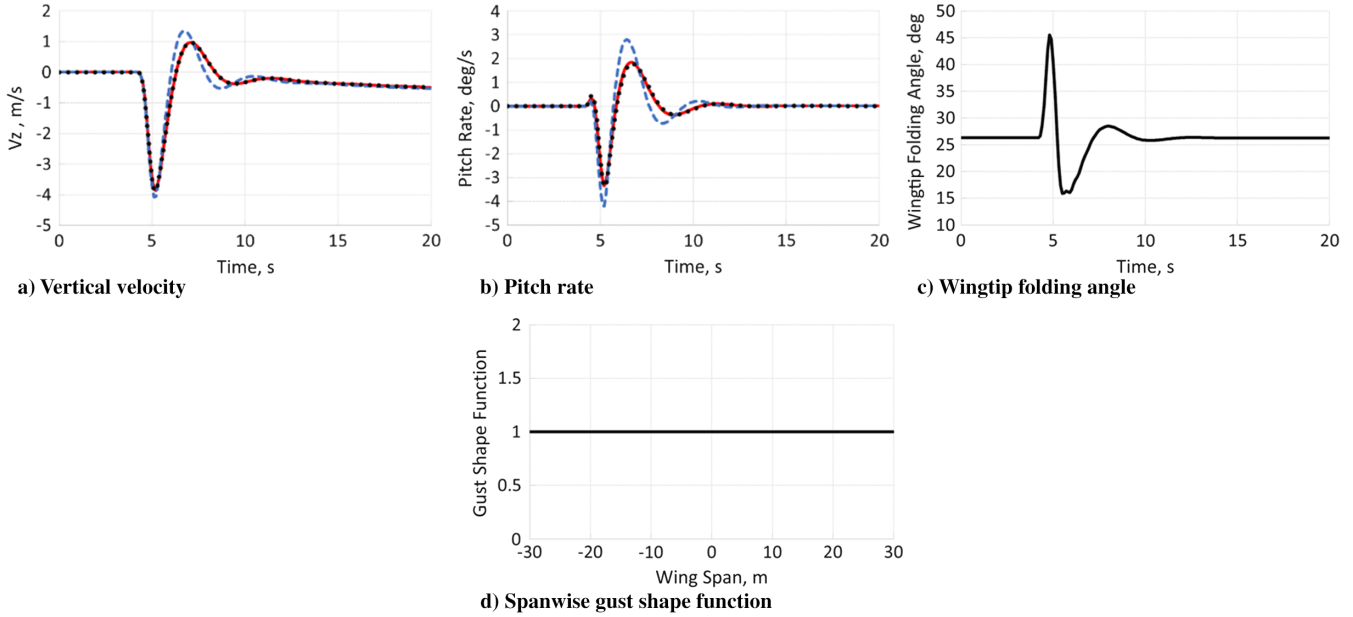

Fig. 9 Dynamic gust response: baseline (black dotted line); fixed hinge (blue dashed line); and free hinge (red solid line).

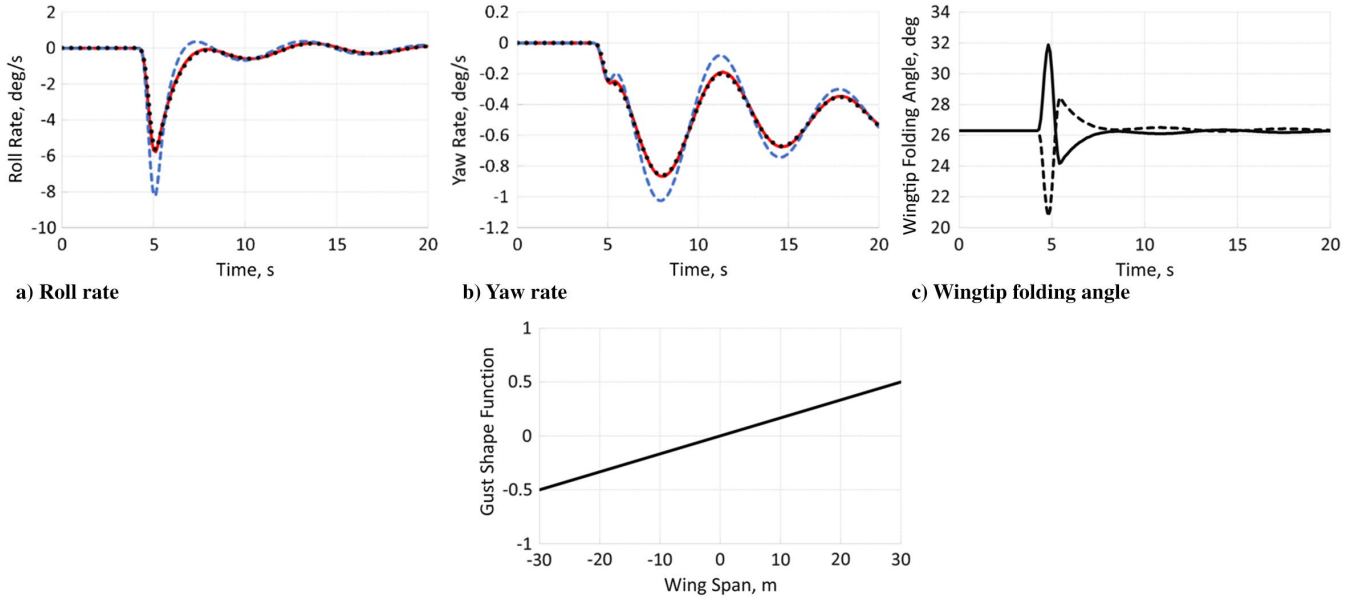

Fig. 10 Dynamic gust response (asymmetric spanwise distribution): baseline (black dotted line); fixed hinge (blue dashed line); and free hinge (red solid line).

the baseline. Lower pitch and altitude variations are observed for the fixed-hinge aircraft.

As regards the response due to the rudder, shown in Fig. 8, the free hinge and the baseline model report higher roll rates but slower yaw rates when compared to the fixed-hinge aircraft. Also, in this case, an asymmetric deflection of the wingtips is observed.

C. Gust Response

This section presents the dynamic response of the free-flying aircraft due to a "1-cosine" gust. Only one gust length of 214 m is considered, and the gust amplitude has been selected according the European Union Aviation Safety Agency regulations [14].

Figure 9 shows the response of the three aircraft in terms of the vertical speed and pitch rate induced by the gust. This latter is considered uniform across the wingspan. As in the previous case, the free-hinge aircraft response is close, if not equal, to the baseline one. The wingtips act as a dynamic damper, reducing the vertical speed and pitch rate experienced by aircraft with respect to the fixed-hinge model. Moreover, Fig. 9b confirms that the fixed-hinge aircraft has a lower short-period frequency.

Similar results are reported in Fig. 10 but for a nonuniform spanwise gust. In this case, the wingtips damp the perturbation introduced by the gust in terms of the roll and yaw rate.

Figure 11 shows the long-term response to a uniform spanwise gust. The same long-period response is observed for the three models, confirming that reported in Fig. 5a.

D. Dynamic Wingtip Release

The SAH wingtip concept is based upon the idea of having the wingtips fixed during the cruise condition in order to maximize the aerodynamic benefits due to the longer span, as well as to release them only when needed, both to reduce the loads or enhance the aircraft maneuverability. A question arises as to what the dynamic response would be of the aircraft induced by the wingtip release. Figure 12 shows some related interesting quantities. As soon as the hinge is released, the wingtips tend to rotate upward to their

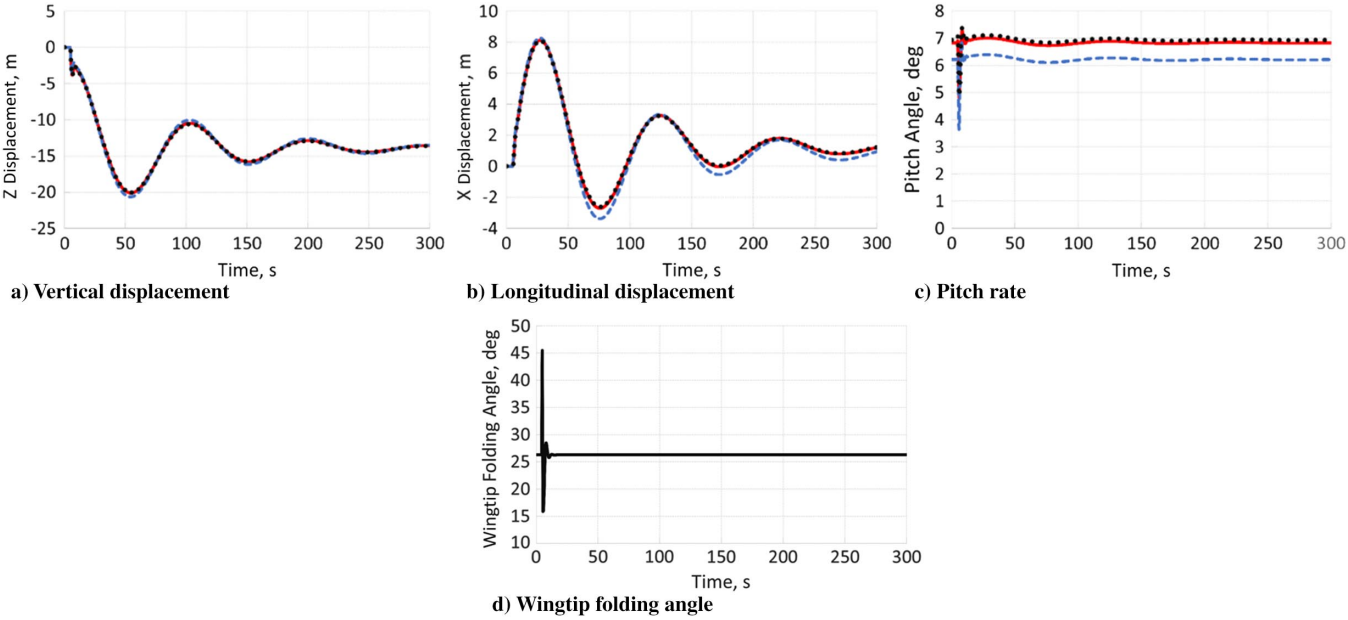

Fig. 11 Dynamic gust response (long-term response): baseline (black dotted line); fixed hinge (blue dashed line); and free hinge (red solid line).

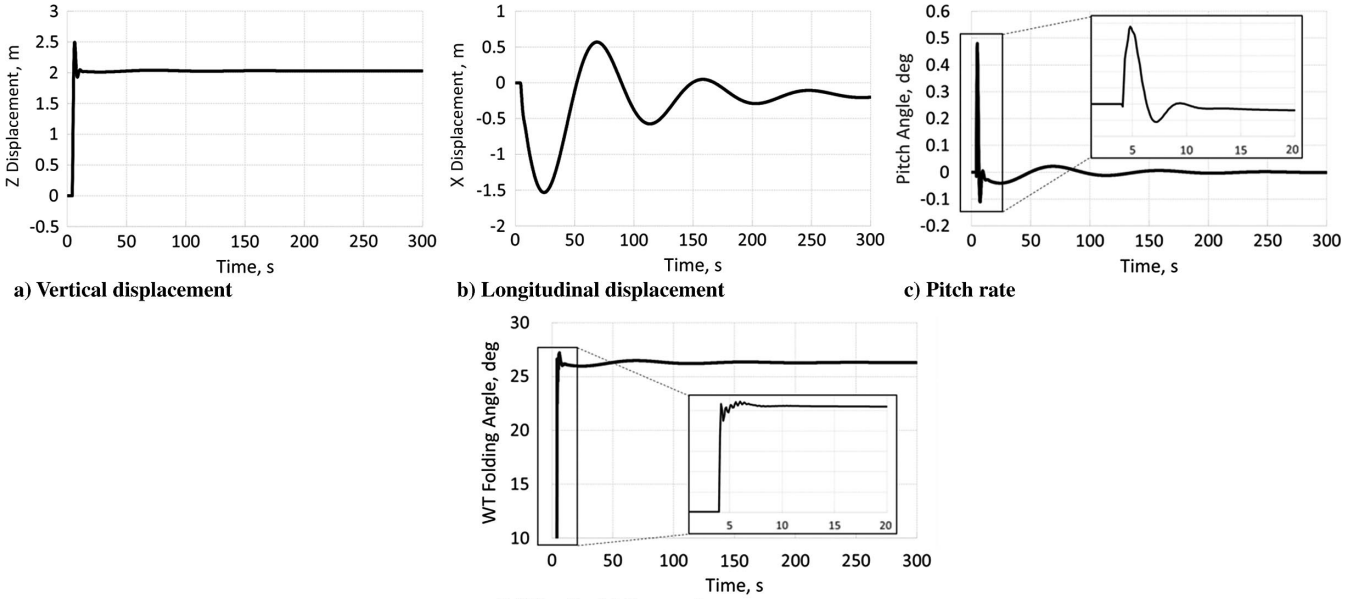

a) Vertical displacement **b) Longitudinal displacement** **c) Pitch rate**

d) Wingtip folding angle

Fig. 12 Dynamic wingtip release response.

free-floating equilibrium positions. This leads to the generation of local negative incremental aerodynamic forces at the tips, which also reflects in a pitchup moment. As a consequence, the wingtip release excites both the short and the long periods. However, such an excitation generated a lower perturbation with respect to the one induced by a gust. Moreover, after the wingtip is released, a variation on the elevator angle is also required in order to balance the pitching moment induced by the tip deflection [16].

IV. Conclusions

A preliminary analysis of the impact of the SAH on the aircraft flight dynamics has been investigated. The results have shown that, despite the 25% increment in span, the free-hinge aircraft has the same handling qualities and dynamic response of the baseline model with no wingtip extension. Such a finding extends the applicability of the SAH, which can be used both as a load reduction device and to alleviate the roll damping increment induced by the longer span. This results in an enhanced aileron authority with a consequent weight savings with respect to the fixed-hinge aircraft, due to the smaller aileron size required.

A free wingtip will passively do whatever it takes to satisfy the condition of a zero hinge moment condition; this results in the tip attitude offloading itself, thus minimizing its impact on the loads and the handling qualities when compared to an aircraft without the wing extension.

Future work will be focused on the introduction of a multibody formulation of the aircraft/wingtip system in order to investigate the impact of the geometric nonlinear effects due to the wingtip deflection on both the aircraft loads and flight dynamics.

References

[1] Castrichini, A., Hodigere Siddaramaiah, V., Calderon, D. E., Cooper, J. E., Wilson, T., and Lemmens, Y., "Preliminary Investigation of use of Flexible Folding Wing-Tips for Static and Dynamic Loads Alleviation," *Aeronautical Journal*, Vol. 121, No. 1235, Jan. 2017, pp. 73–94. https://doi.org/10.1017/aer.2016.108

[2] Castrichini, A., Hodigere Siddaramaiah, V., Calderon, D. E., Cooper, J. E., Wilson, T., and Lemmens, Y., "Nonlinear Folding Wing Tips for Gust Loads Alleviation," *Journal of Aircraft*, Vol. 53, No. 5, Sept. 2016, pp. 1391–1399. https://doi.org/10.2514/1.C033474

[3] Castrichini, A., Cooper, J. E., Wilson, T., Carella, A., and Lemmens, Y., "Nonlinear Negative Stiffness Wing-Tip Spring Device for Gust Loads Alleviation," *Journal of Aircraft*, Vol. 54, No. 2, 2017, pp. 627–641. https://doi.org/10.2514/1.C033887

[4] Cheung, R. C. M., Rezgui, D., Cooper, J. E., and Wilson, T., "Testing of a Hinged Wingtip Device for Gust Loads Alleviation," *Journal of Aircraft*, Vol. 55, No. 5, Sept. 2018, pp. 2050–2067, https://doi.org/10.2514/1.C034811

[5] Wilson, T., Azabal, A., Castrichini, A., Cooper, J. E., Ajaj, R., and Herring, M., "Aeroelastic Behaviour of Hinged Wing Tips," *International Forum on Aeroelasticity and Structural Dynamics*, IFASD-2017-216, 2017.

[6] Saltari, F., Riso, C., De Matteis, G., and Mastroddi, F., "Finite-Element-Based Modeling for Flight Dynamics and Aeroelasticity of Flexible Aircraft," *Journal of Aircraft*, Vol. 54, No. 6, 2017, pp. 2350–2366. https://doi.org/10.2514/1.C034159

[7] Canavin, J. R., and Likins, P. W., "Floating Reference Frames for Flexible Spacecraft," *Journal of Spacecraft and Rockets*, Vol. 14, No. 12, Dec. 1977, pp. 724–732. https://doi.org/10.2514/3.57256

[8] Meirovitch, L., and Tuzcu, I., "The Lure of the Mean Axes," *Journal of Applied Mechanics*, Vol. 74, No. 3, 2007, pp. 497–504. https://doi.org/10.1115/1.2338060

[9] Waszak, M. R., Buttrill, C. S., and Schmidt, D. K., "Modeling and Model Simplification of Aeroelastic Vehicles: An Overview," NASA TM 107691, 1992.

[10] Looye, G., "Integration of Rigid and Aeroelastic Aircraft Models Using the Residualised Model Method," *International Forum on Aeroelasticity and Structural Dynamics*, CEAS/DLR/AIAAA, 2005, Paper IF-046.

[11] Kier, T., "Comparison of Unsteady Aerodynamic Modelling Methodologies with Respect to Flight Loads Analysis," *AIAA Atmospheric Flight Mechanics Conference and Exhibit*, AIAA Paper 2005-6027, 2005. https://doi.org/10.2514/6.2005-6027

[12] Albano, E., and Rodden, W. P., "A Doublet-Lattice Method for Calculating Lift Distributions on Oscillating Surfaces in Subsonic Flows," *AIAA Journal*, Vol. 7, No. 2, 1969, pp. 279–285. https://doi.org/10.2514/3.5086

[13] Rodden, W. P., and Johnson, E. H., "MSC/NASTRAN Aeroelastic Analysis: User's Guide," MSC Software, Newport Beach, CA, 1994.

[14] Certification Specifications for Large Aeroplanes CS-25, European Union Aviation Safety Agency, 2007, https://www.easa.europa.eu/document-library/certification-specifications/cs-25-amendment-23.

[15] Roger, K. L., "Airplane Math Modeling Methods for Active Control Design," *AGARD Structures and Materials Panel*, AGARD CP-228, Neuilly-Sur-Seine, France, 1977, pp. 4–11.

[16] Castrichini, A., Wilson, T., and Cooper, J. E., "On the Dynamic Release of the Semi Aeroelastic Hinge Wing-Tip Device," *RAES 6th Aerospace Structures Design Conference*, Royal Aeronautical Soc., 2018, Paper D.2.